Science of Sintering, **57** (2025) 53-68

https://doi.org/10.2298/SOS240502023Y

UDK: 53.086; 676.017.2; 692.533.1

Investigation of Microstructural, Mechanical and Tribological Properties of NiTi/nB_4C Metal Matrix Composites Produced by Spark Plasma Sintering

Taha Alper Yilmaz[1*)], Ufuk Tasci[1], Naci Arda Tanis[2], Hakan Gokmese[3], Muharrem Kocak[2], Bulent Bostan[4]

[1]Department of Technical Sciences Vocational School, Gazi University, Ankara, 06374, Turkey.

[2]Department of Metallurgical and Materials Engineering, Kırıkkale University, Kırıkkale, 71451, Turkey.

[3]Department of Mechanical Engineering, Necmettin Erbakan University, Konya, 42140, Turkey.

[4]Department of Metallurgical and Materials Engineering, Gazi University, Ankara, 06374, Turkey.

Abstract:

In this paper, it was aimed to improve the microstructure, mechanical and tribological properties of composite samples according to the alloy by adding 0.25%, 0.5% and 1% nano B_4C to NiTi shape memory alloy. A 3D ball mixer device was used to prepare composite powders and the samples were produced by Spark Plasma Sintering technique. FE-SEM/EDS and XRD were used for microstructure and phase characterization, nanoindentation to determine mechanical properties, and pin-on disc wear device to determine wear properties. It was determined that with the increase in the reinforcement ratio added to the NiTi alloy, nB4C ceramic particles settled at the grain boundaries and the hardness value of the 1% nB_4C (334 HV) sample with the highest hardness increased significantly by 30% unreinforced NiTi alloy (264 HV).

Keywords*: Microstructure; Mechanical properties; Composites.*

1. Introduction

NiTi alloys are used in biomedical, automotive, space and aviation industries due to their unique properties such as shape memory and pseudoelasticity (PE). In addition, its superelastic property allows it to be separated from many different alloys. When these materials are subjected to a thermo-mechanical process, they are in the class of shape memory alloys because they keep their untreated state in their memory. The characteristic feature such as shape memory can be defined as deformation under external force at a specific temperature and return to its original shape after being heated to the transformation temperature. In this case, it is due to the thermoelastic transformation between the high temperature austenitic B2 phase and the low temperature B19' martensite phases [1–4]. During the cooling of the NiTi alloy, the martensitic transformation starts at the temperature martensite start (M_s) and is completed at the temperature martensite finish (M_f). During the heating cycles, reverse

*) **Corresponding author:** tahaalperyilmaz@gmail.com; tahaalperyilmaz@gazi.edu.tr

martensitic transformation takes place. This transformation ends with the austenite finish temperature, which begins to transform into the B2 phase. The two most important factors affecting phase transformation are stress and the Ni-Ti ratio [5,6]. It is known from the studies that the wear resistance of NiTi alloys is basically related to the PE property. In order to increase the wear resistance of this alloy, the matrix phase is transformed into martensite by applying a deformation to the material. Thus, the contact area between the surfaces increases and the stress ratio on the surface decreases, which leads to an increase in wear resistance. In addition, after the applied deformation process, a reverse phase transformation occurs. The deformation is fully or partially recovered, and the amount of strain stored in the matrix decreases [7–9]

The increase in wear resistance in metal matrix composites (MMC) is generally associated with hardness. It is known that ceramic particles reinforced into the matrix increase the hardness of the material by forming a composite [10]. The effects on wear resistance by adding ceramic reinforcements such as TiN [11], TiC[12], SiC[13], Al_2O_3[14], CNT [15] into NiTi alloys have been reported in previous studies. However, the number of nano-reinforced composite studies is limited. The nano size of the ceramic phase reinforced into the matrix phase increases the interaction of the particles with the dislocations and thus paves the way for the development of composites with higher mechanical properties than the particles added in micro size [16–18]. The most used methods for producing MMCs are casting and powder metallurgy processes. The reinforced ceramic particle is mixed into the liquid in the casting method. However, it has been reported in many publications that the reinforcement material cannot mix homogeneously in the liquid metal mixing process and agglomeration occurs [19–21].

In the powder metallurgy (PM) method, there are different processes to produce composites. The most important and known of these processes are hot pressing (HP) [22], cold isostatic pressing (CIP) [23], hot isostatic pressing (HIP) [24]and spark plasma sintering (SPS) [25] techniques. Especially in the SPS method, the harmony between the matrix and the ceramic reinforcement is provided very well. This is because the temperature rises to very high levels with the high electrical voltage formed between the contacting powder particles. Thus, excellent matrix-reinforcement interface compatibility is achieved [26]

This study aimed to produce composite samples by adding nano B_4C (nB_4C) ceramic reinforcement into NiTi shape memory alloy at different rates. The literature search found only one publication on producing B_4C-reinforced composite material with NiTi matrix [2]. Our study focused on the effect of nano-ceramic reinforcement on the matrix by examining the microstructure and wear properties with composite fabrication using different reinforcement ratios. It is aimed to increase the hardness by decreasing the relative density of NiTi composite materials used in critical sectors such as aerospace and aerospace, as well as to improve their tribological properties and expand their use.

2. Materials and Experimental Procedures

2.1 Preparation of composite powders

Equiatomic and pre-alloyed NiTi powders as matrix materials were obtained from Nanoval Company. NiTi alloy powders used in experimental studies are spherical and 10 μm in size. nB_4C 55 nm sized ceramic particles reinforced into NiTi matrix were used at 0.25, 0.5 and 1 wt% ratios. Fig. 1 shows FE-SEM images of NiTi alloy powders and nB_4C ceramic particles used as matrix phase. When the figure is examined, images of spherical NiTi alloy powders and complex shaped nB_4C powders at different magnifications are seen.

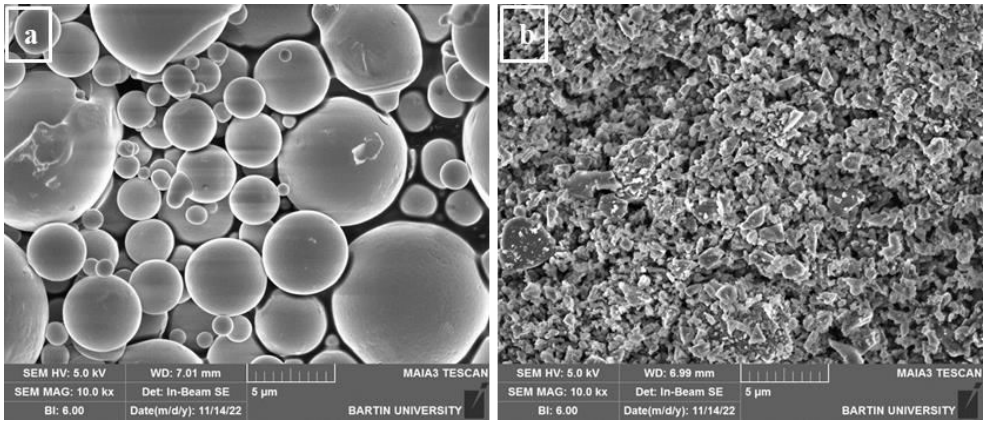


Fig. 1. a) Equiatomic spherical NiTi powders, b) complex shaped nB_4C powders.

The mixing process of matrix NiTi alloy and nB_4C ceramic powders prepared in different ratios were carried out to produce composite powders in a 3D high-energy ball mixer. The mixing process parameters are given in Table I.

Tab. I Mixing parameters of composite powders.

Powder/Ball ratio	1/5	
Cycle (rpm)	X axis: 500	Y axis: 200
Duration (h)	4	
Ball type	ZrO_2	
Atmosphere	Argon (Ar)	

FE-SEM images in which the nB_4C ceramic particles are homogeneously dispersed on the surface without changing their spherical morphology in the NiTi matrix in the mixing process at different rates are given in Fig. 2.

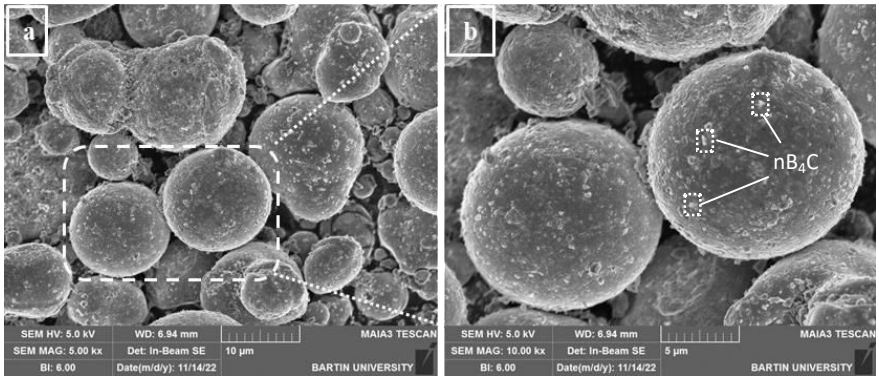


Fig. 2. FE-SEM images of mixed composite powders at different magnifications.

2.2 Production of composite powders by SPS process

The production process of non-reinforced NiTi alloy and composites at 0.25, 0.5 and 1 wt% nB_4C ratios was carried out with the SPS process. SPS process parameters are given in Table II. The optimum temperature and pressure values were determined after the literature review and preliminary studies, and the production of composites and unreinforced NiTi alloy was carried out.

Tab. II SPS process parameters for the production of NiTi/nB_4C composites.

Final processing temperature (°C)	900	
Heating rate (°C/min)	100	
Pressing pressure (MPa)	Pre-Pressing: 5	Pressing: 35
Duration (min.)	15	
Atmosphere	Nitrogen (N_2)	

2.3 Microstructure and mechanical analysis

The mesh produced by the SPS process. Standard sanding and polishing metallographic pre-treatments were applied for the microstructure investigations of 0.25, 0.5 and 1 wt% nB_4C reinforced NiTi matrix composites and the unreinforced NiTi alloy. Polished surfaces of samples vol. Etched with 5% HF, 15% HNO_3 and ethyl alcohol. FE-SEM, EDS and mapping processes were carried out to analyze the microstructure of the prepared samples and the chemical composition of the phases formed in the matrix. XRD (Bruker D8 ADVANCE) analyses were performed between 20 – 90° 2θ angles to determine the phases formed in the matrix of the composite samples after the sintering process and the composition of the phases. Brinell hardness measurements were taken according to ASTM E10-15 standard to examine the mechanical properties of the composite samples for which XRD analyses were performed.

2.4. Wear Tests

In order to analyses the wear properties of nB_4C reinforced NiTi matrix composites, the microstructure and mechanical properties of which were examined, the pin-on disc wear method on the Anton Paar TRB^3 device according to ASTM G99-05 standard was applied on the Al_2O_3 with a diameter of 6 mm at a speed of 0.19 mm/s, and exposed to a 20 N load at a distance of 1500 meters. has been left. The wear behaviour of the samples after the wear process was evaluated by determining the mass loss and taking the surface topography from the 3D Profilometer device (Filmetrics Profilm3D-200). During the processes carried out for the samples where wear tests were carried out, the ball's wear scar areas, width measurement and volume losses were evaluated using the ProfilmOnline software available on the 3D Profilometer device. Calculation of the specific wear rate was carried out according to Eq. 1.:

$$\omega = \left(\frac{V}{(L\ x\ N)}\right) \qquad (1)$$

where, V is wear volume, L is sliding distance and N is load. In addition, the worn surface imaging of all samples was made with FE-SEM and the properties formed on the surface after wear were determined.

3. Results and Discussion

3.1. Microstructure and phases characterization

Microstructure images obtained with B_4C ceramic particle reinforcement in NiTi equiatomic alloy powders without reinforcement, reinforced at the rates of 0.25, 0.5 and 1% are given in Fig. 3. It has been determined that the reinforcement material in the alloy generally forms at grain boundaries and there is no change in grain sizes.

FE-SEM images of unreinforced NiTi alloy and nB_4C-reinforced NiTi composites are given in Fig. 3. When the FE-SEM images are examined, it is seen that the grains are sintered in the neck regions of the composites without nB_4C reinforcement.

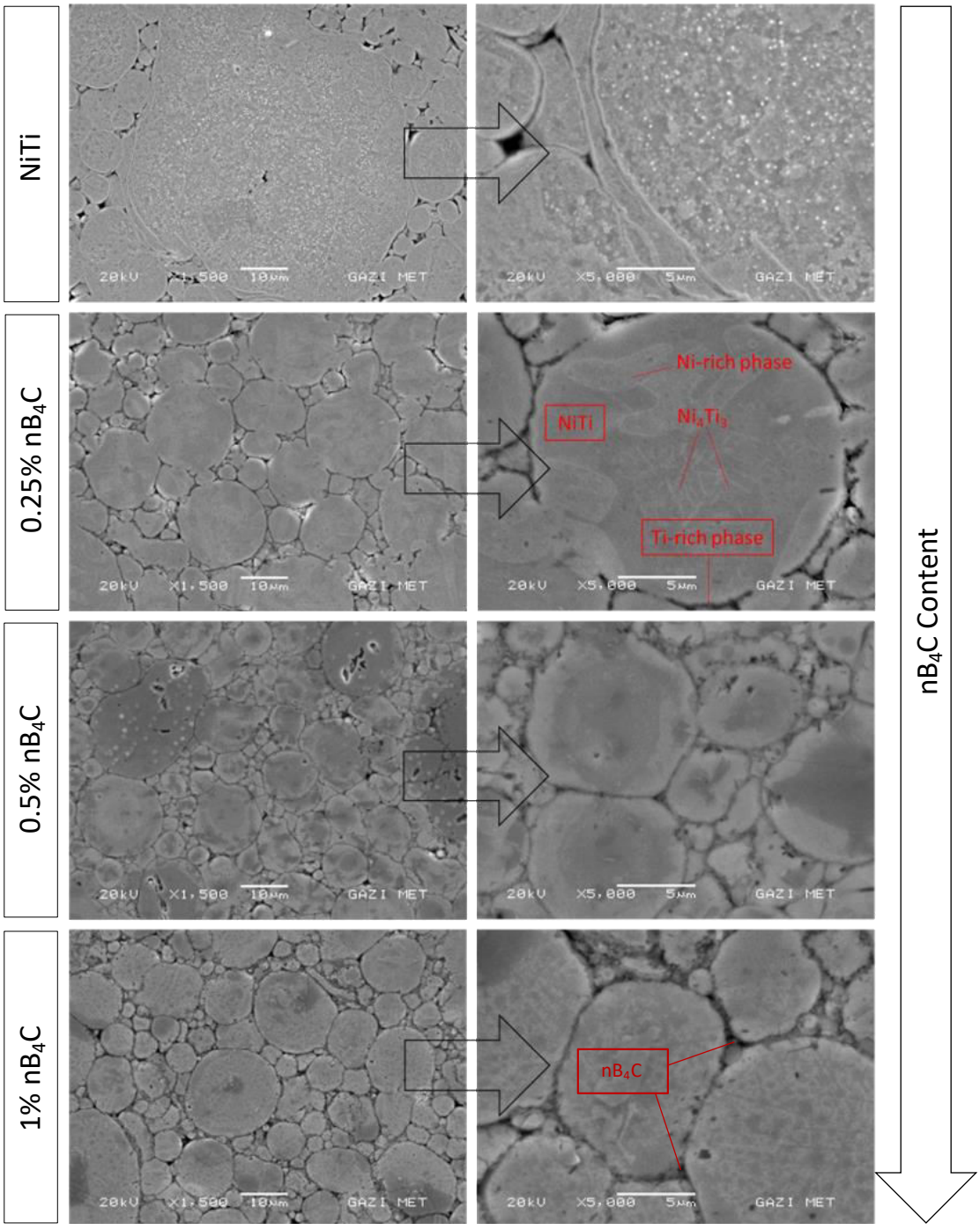


Fig. 3. FE-SEM image of unreinforced and nB_4C reinforced NiTi composites.

When the FE-SEM images given according to the increasing reinforcement ratio in Fig. 3 were analyzed, it was determined that the nano B_4C particles settled around the grains because mixing in the ball mill prevented the formation of the neck region in the sintering region. It was determined that the dark regions increased between the grain boundaries, whereas the neck region formed at the grain boundaries decreased with the increasing reinforcement ratio. B_4C particles were pressed onto the surface of NiTi particles by creep during compaction and heating in the SPS. It has been observed that the reason for this is that B_4C particles with a melting temperature of 2350 °C form a thermally stable barrier at the temperature of the NiTi

matrix grains sintered at 900 °C during the SPS process. However, it cannot be said that the sintering has yet to be fully realized here. Namini et al. in their study on the production of Ti-matrix B_4C reinforced composites with spark plasma, they examined the effects of the B_4C ratio on sintering behavior and found that sintering around the grain becomes more difficult as the ratio of B_4C particles increases [27].

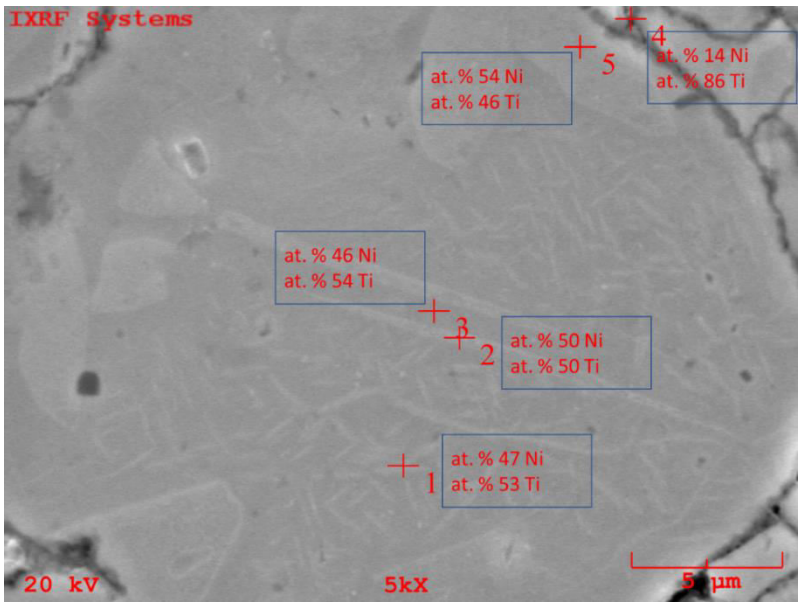


Fig. 4. Point EDS analysis of 0.25% nB_4C reinforced NiTi matrix composite.

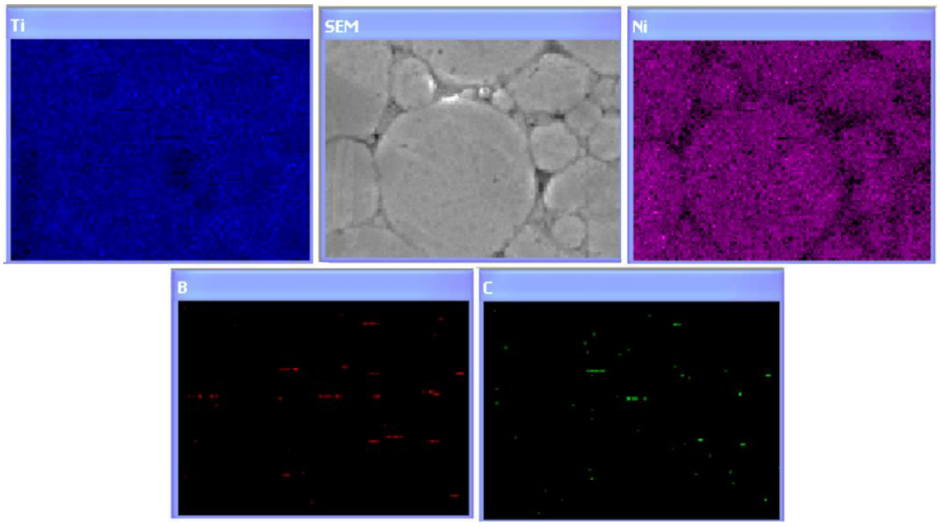


Fig. 5. Mapping image of 1% nB_4C reinforced composite sample.

The point EDS analysis taken from the sample produced after the SPS process of the 0.25% B_4C reinforced NiTi matrix composite given in Fig. 4. examined how the NiTi grain was affected during the SPS process. In the examinations, it was observed that the grain carried the NiTi phase, which is the phase structure before the sintering process. The reason for this is that due to the low sintering time in the SPS process, there is not enough time for the unstable diffusion between Ni and Ti atoms, and thus the NiTi phase preserves its structure before the sintering process. This phenomenon is one of the advantages of the SPS method over

traditional sintering methods. With the increasing sintering time in traditional sintering methods, due to Ni-Ti diffusion in the grain, the equiatomic NiTi phase cannot preserve its structure, and the more stable Ni_3Ti and Ti_2Ni phases become effective. The samples require secondary heat treatment to show shape memory and superelasticity properties in this case. At the grain boundaries, diffusion between Ti and Ni atoms has occurred due to the effect of temperature and time. At the same time, the Ti-rich phase is dominant in the dark regions of the grain boundaries, while the ratio of Ni element in the light gray phase located near the grain boundary is higher than the Ti element Fig. 5 shows the mapping image of 1% nB_4C reinforced NiTi alloy.

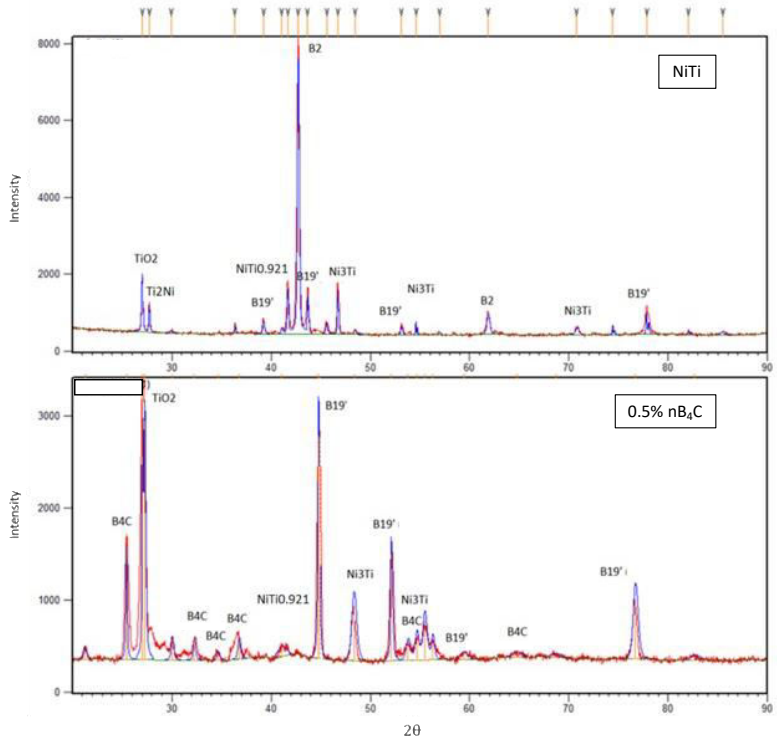


Fig. 6. XRD patterns of unreinforced NiTi alloy and 0.5% nB_4C reinforced NiTi matrix composite.

Fig. 6 shows XRD analyses of unreinforced NiTi alloy and 0.5% nB_4C reinforced NiTi matrix composite. XRD analyzes were performed at room temperature. When the XRD analysis of the NiTi alloy is examined, it is seen that the peaks of the B2 phase, which is the austenite phase, are dominant. In the composite sample, the dominant phase is the B19 martensite phase. In addition, the peaks of Ni_3Ti and TiO_2 phases are observed in both structures [28]. Although the sintering time is very short, the reason for this can be explained by the liberation of Ti atoms at the grain boundary and the oxidation of the free Ti atoms when removed from the argon atmosphere. The Ni_3Ti phase, on the other hand, is the transformation of the Ti atoms moving to the grain boundaries into the Ni_3Ti phase, which is the stable phase in the Ti-Ni alloy system in the region where Ti decreases. nB_4C peaks are also seen in the composite sample. When we evaluate both NiTi alloy and nB_4C-reinforced NiTi alloys together, it shows that nB_4C nanoparticles are the trigger for the formation of the martensite phase and transform into a martensite structure at room temperature in the composite sample compared to NiTi in the austenite phase in the unreinforced state. From this, nB_4C nanoparticles increase the austenite transition temperature.

3.2. Density and Nanoindentation Tests

Density tests of composites produced with NiTi alloy and reinforced with 0.25, 0.5, and 1% nB_4C ceramic particles were carried out using the Archimedes principle. The density value of the unreinforced NiTi alloy was determined to be 6.34 g/cm^3. A decrease in density values was observed with increasing reinforcement rate. The density value of the composite produced with 1% nB_4C reinforcement, which has the highest reinforcement value, gave the lowest value. This is due to the density value of nB_4C (2.52 g/cm^3). nB_4C reduces the density of the composite with increasing reinforcement ratio, allowing it to be lighter. Fig. 7 shows the change in density values depending on the increasing reinforcement rate.

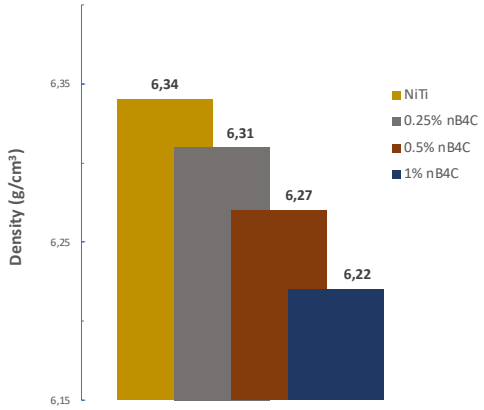


Fig. 7. Experimental densities of NiTi alloy and nB_4C reinforced composites.

The nanoindentation technique was used to determine composites' local mechanical and pseudoelasticity properties with different reinforcement ratios bulked by the SPS method. Fig. 8 shows the load and depth curves of composites produced with unreinforced NiTi alloy and nB_4C reinforcement at 0.25, 0.5 and 1% by weight. Hardness values in Vickers (HVIT), modulus of elasticity (E*) and penetration depth of the penetrating tip (hmax), epsilon, elastic, plastic and total energies are calculated respectively in $W_{elas.}$, $W_{plas.}$ and $W_{tot.}$ values are given in Table III.

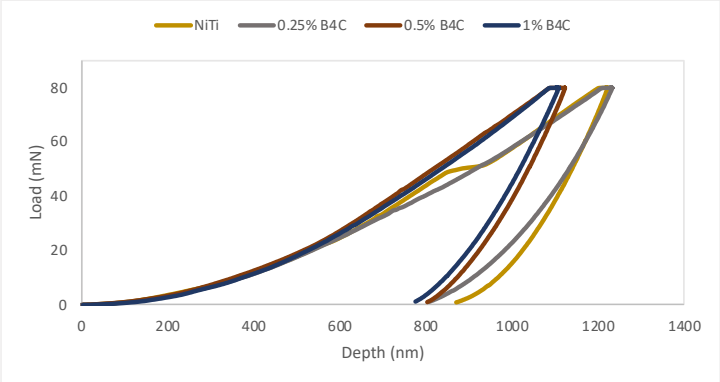


Fig. 8. Nanoindentation test of NiTi alloy and nB_4C reinforced composites.

When the results given in Table III were examined, it was determined that there was an increase in HVIT nano hardness values with an increasing reinforcement ratio. This situation is likely because, with the increasing reinforcement ratio, nB_4C particles with high hardness

are distributed homogeneously within the grains and at the grain boundaries, acting as a barrier preventing dislocation movements [29,30]. In addition, the increase in nickel-rich and titanium-rich stable intermetallic phases in the composite samples was a factor that increased the hardness.

Tab. III Mechanical properties of NiTi alloy and nB_4C reinforced composites.

	NiTi	**%0.25 nB_4C**	**%0.5 nB_4C**	**%1 nB_4C**
HVIT	264	271	326	344
E* (GPa)	68.447	58.695	73.318	70.377
h_{max} (nm)	1222.218	1233.625	1123.863	1109.425
Epsilon	0.728	0.727	0.733	0.739
$W_{elas.}$(pj)	10.533	13.115	10.481	11.059
$W_{plas.}$(pj)	27.182	24.576	23.878	21.025
$W_{tot.}$(pj)	37.716	37.692	34.359	32.085

Since boron carbide has a covalent bond, its elasticity modulus and hardness values are high compared to metals. According to the mixing rule, an increase in elastic modulus and hardness is expected with an increasing reinforcement ratio. It was determined that there was a partial increase in elasticity modulus values with increasing reinforcement ratio, but there was no significant increase. Since it is thought to keep the nB_4C reinforcement rates low in the NiTi alloy and thus increase the mechanical properties, the rates were kept at such low values. It was determined that the sinking depth values decreased with increasing reinforcement ratio. It was determined that epsilon values increased with the increase in reinforcement rate. The work done was determined by measuring the deformation in terms of energy. When the table was examined, it was determined that the plastic and total deformation energy amounts gradually decreased with increasing reinforcement ratio. Since elasticity and hardness rates are directly related to wear behavior, these analyses were carried out, and subsequent wear tests were carried out.

It is known that the unreinforced NiTi alloy is in the B2 austenitic phase at room temperature. In a study, it was stated that the stresses occurring in the contact area of the indenter in the nanoindentation process would have the highest value and therefore, for the sample with an austenitic phase, plastic deformation occurs in the region closest to the indenter and a transition from austenite to martensite may occur due to the effect of stress as the tip advances [31].

3.3. Wear Properties and Worn Surface Morphology

A wear test was applied to determine the tribological properties of NiTi alloy and composite samples reinforced with nB4C at different rates. After the wear test, all samples friction coefficient-distance curves were determined to determine the wear mechanism and properties. Then, characterization processes were carried out by detecting post-wear surface features with FE-SEM and 3D profilometer devices. Fig. 9 shows the friction coefficient-distance curves of composites produced by reinforcing NiTi alloy and 0.25%, 0.5%, and 1% nB_4C, respectively.

When the friction coefficient-distance curves in Fig. 9 are examined, it is determined that the COF value of the unreinforced NiTi alloy is approximately 0.6. It is seen that there is a fluctuation in the friction coefficient with 0.25% nB_4C reinforced into NiTi. The resulting friction coefficient started low at first and then continued to increase. It is thought that ceramic-ceramic surface encounters on the surface together with the Al_2O_3 ball used as a pin may trigger this situation. It was observed that the COF value decreased to the range of 0.4-

0.5, with the reinforcement ratio being 0.5%, respectively. When the 1% NiTi composite sample with the highest nB_4C reinforcement ratio was examined, it was observed that the average COF value was at its lowest, and thus, the increasing reinforcement ratio caused a decrease in the friction coefficient values. In this study, as in many other studies, this situation increases the hardness and strength of the composites developed by increasing the ratio of nB4C ceramic reinforcement in the matrix phase, thus causing a significant decrease in COF values [32,33]. The specific wear rates of unreinforced NiTi alloy and nB4C reinforced composite samples are shown in Fig. 10.

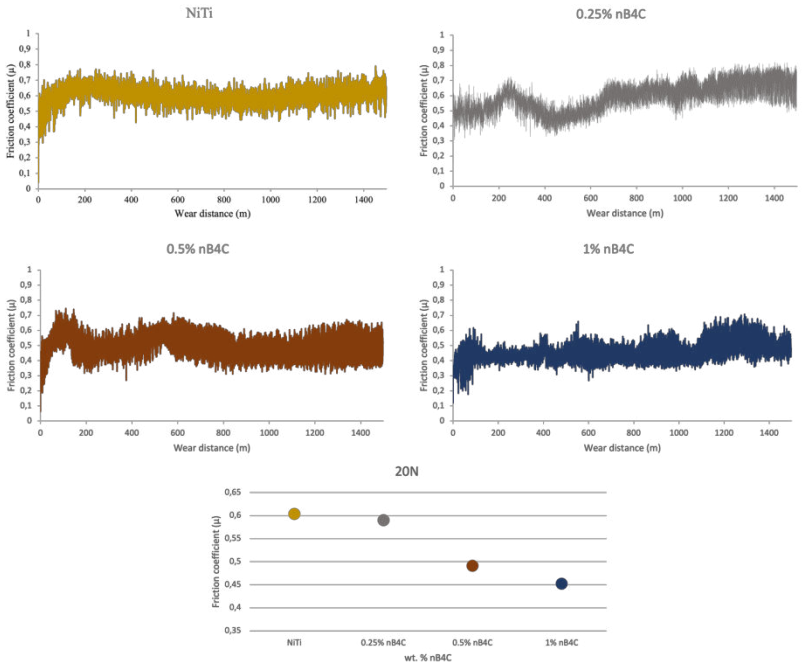


Fig. 9. Friction coefficient – distance curves of NiTi and nB_4C reinforced composite samples.

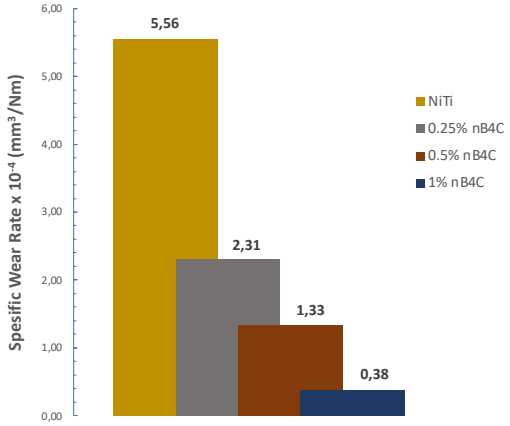


Fig. 10. Specific wear rates of NiTi and nB_4C reinforced composite samples.

In order to determine the specific wear rates of all samples, the volume in the worn surface areas displayed on the 3D profilometer device was calculated with the ProfilmOnline software. When the results are examined, the increasing hardness values increasing the reinforcement ratio in the composites produced caused the wear rates to decrease. As it is

known, there is an inverse proportion between hardness and wear rate [34,35]. Similar to the literature, it was determined in this study that the strength improved with increasing nB_4C supplementation significantly reduced the wear rate. FE-SEM images of worn surface morphologies are shown in Fig. 11 to examine the mechanisms of materials formed on the surface after wear.

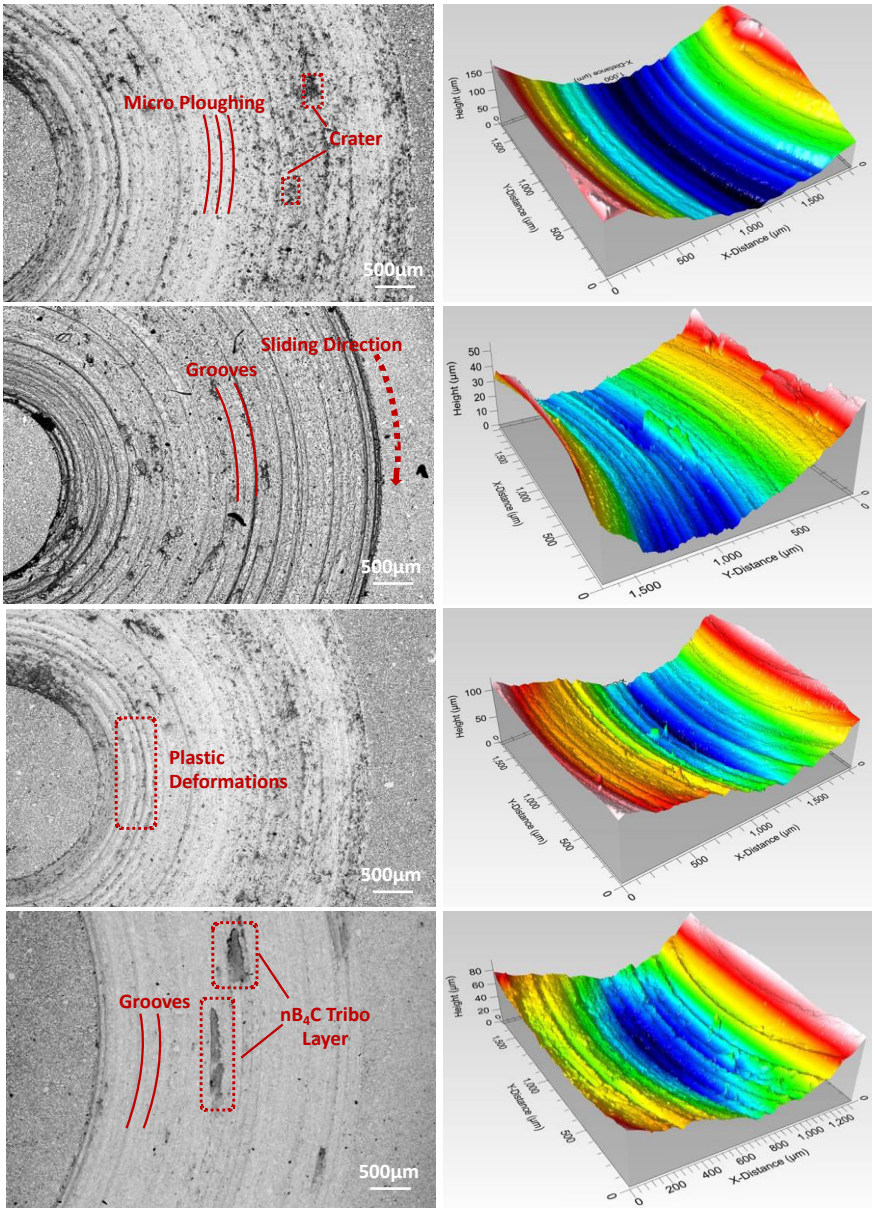


Fig. 11. Worn surfaces and 3D isometric images of NiTi and nB_4C reinforced composite.

When the FE-SEM images of the worn surface in Fig. 11 are examined, it is seen that the wear surface width is the highest in the unreinforced NiTi alloy. In all samples, the sliding direction explains the smallest amount of worn surface in the sample with the highest reinforcement ratio (1%). It was determined in the FE-SEM images that an abrasive wear mechanism generally occurred in all samples. It has been observed that deep grooves, scratches, craters and plastic deformation zones occur in the unreinforced NiTi alloy. It can be seen that the number of grooves in the 3D isometric image is very high. As expected, it was

determined that the highest rate of wear marks occurred in the unreinforced NiTi alloy, which has the lowest hardness amount. When the composite sample with a 0.25% nB_4C reinforcement ratio is examined, it is seen that deep scratches are reduced compared to the unreinforced NiTi alloy. When the 3D isometric image is examined, the depth after wear is thought to decrease due to the increase in hardness. When the FE-SEM image of the composite sample produced with a 0.5% nB_4C reinforcement rate was examined, it was determined that the wear scar width was further reduced compared to the 0.25% nB_4C reinforced composite sample. In the 3D isometric image, it was determined that the wear depth of the plastic deformation zones decreased with increasing hardness value compared to the sample containing less reinforcement. Finally, it was determined that the composite sample produced with a 1% nB_4C reinforcement rate was the sample with the minor wear marks in the worn surface image and the sample with the minor wear depth in the 3D isometric image. It is thought that the dominant wear mechanism in all samples is abrasive wear and that it causes plastic deformation due to the high 20 N load applied. As the nB_4C reinforcement ratio increases, a decreasing wear scar width is observed in the 0.25%, 0.5% and 1% composite samples, respectively. That can be explained by the increase in hardness values with increasing reinforcement ratio in composite samples. Increasing the hardness is possible by distributing the nB_4C reinforcement homogeneously within the NiTi matrix and increasing the ratio of Ti_2Ni and $TiNi_3$ stable intermetallic phases in the matrix as the reinforcement ratio increases [36].

4. Conclusion

The main results of the research are summarized below:

- When the FE-SEM images of the samples produced with NiTi alloy and nB_4C reinforcement were examined, flat powders seen in the mechanical alloying process were not detected in the powder grains, with the process carried out in the 3D ball mixer. In conclusion, the XX material used as the reservoir does not change the grain morphology and is more efficient for homogeneous mixtures. It was also determined that the SPS technique did not affect the grain size during sintering. Diffusion, which occurs over time and temperature in traditional powder metallurgy methods, occurred in small amounts due to the short sintering time in SPS production, and the Ni_4Ti_3 precipitates in the pre-alloyed powders remained in the matrix. Nickel-rich areas inside the grains and Titanium-rich areas towards the outside of the grains have been detected. In EDS analyses, Ni_3Ti and $NiTi_2$ intermetallic phases and B2 and B19 phases were detected.
- When the XRD patterns were examined, it was determined that the B2 phase was dominant in the unreinforced NiTi alloy and the B19 phase was dominant in the composite sample with 0.5% nB_4C reinforcement. In addition, it is thought that the Ti atoms located at the grain boundaries in both samples from the TiO_2 phase under atmospheric conditions after sintering.
- When the density values of all samples were examined, it was determined that there was a decrease in the values as the nB_4C reinforcement ratio increased. When the hardness values measured by nanoindentation are examined, increasing the reinforcement ratio increases the hardness values. Additionally, it has been determined that the energy the materials store (in terms of toughness) decreases with increasing hardness.
- When the wear test samples were applied to all samples and examined, it was determined that increasing the reinforcement ratio increased the hardness and that the distortion affected the friction coefficient values, causing decreasing values with increasing reinforcement.

- When the surface properties after wear were examined, it was determined that the increasing hardness values with the reinforcement ratio had a gradually decreasing effect on the worn surface and the wear scars decreased. When the 3D isometric images were examined, it was determined that as the reinforcement ratio increased, the wear depth decreased, and thus, the wear rate decreased.

Acknowledgments

This work was supported by the Gazi University Scientific Research Projects Coordination Unit. Project Number: 6178-07/2020-10.

ORCID numbers:

Taha Alper YILMAZ, https://orcid.org/0000-0002-4316-6890
Ufuk TAŞCI, https://orcid.org/0000-0002-8577-443X
Naci Arda TANIŞ, https://orcid.org/0000-0001-5547-9790
Hakan GÖKMEŞE, https://orcid.org/0000-0003-0053-8444
Muharrem KOÇAK, https://orcid.org/0000-0001-6350-6197
Bülent BOSTAN, https://orcid.org/0000-0002-6114-875X

5. References

1. Ye HZ, Li DY, Eadie RL. Influences of porosity on mechanical and wear performance of pseudoelastic TiNi-matrix composites. J Mater Eng Perform, 10 (2001) 178–185. https://doi.org/10.1361/105994901770345196
2. Velayatipour O, Nikzad L, Farvizi M. B4C reinforced NiTi-based composites: Microstructure and wear performance. Int J Appl Ceram Technol, 20,3 (2023) 1667–1680. https://doi.org/10.1111/ijac.14286
3. Otsuka K, Ren X. Physical metallurgy of Ti-Ni-based shape memory alloys. Prog Mater Sci, 50, 5 (2005) 511–678. https://doi.org/10.1016/j.pmatsci.2004.10.001
4. Singh R, Sharma AK, Sharma AK. Nickel-titanium based nanocomposites for orthopedic applications: the effects of reinforcements. Dig J Nanomater Biostruct, 16, 4 (2021) 1501–1518. https://doi.org/10.15251/djnb.2021.164.1501
5. Gallardo Fuentes JM, Gümpel P, Strittmatter J. Phase Change Behavior of Nitinol Shape Memory Alloys. Adv Eng Mater, 4 (2002) 437–452. https://doi.org/https://doi.org/10.1002/1527-2648(20020717)4:7<437::AID-ADEM437>3.0.CO;2-8
6. Farvizi M, Akbarpour MR, Ahn DH, Kim HS. Compressive behavior of NiTi-based composites reinforced with alumina nanoparticles. J Alloys Compd., 688, 15 (2016) 803–807. https://doi.org/10.1016/j.jallcom.2016.06.299
7. Zheng D, Li R di, Yuan T chui, Xiong Y, Song B, Wang J xing, et al. Microstructure and mechanical property of additively manufactured NiTi alloys: A comparison between selective laser melting and directed energy deposition. J Cent South Univ., 28 (2021) 1028–1042.

https://doi.org/10.1007/s11771-021-4677-y
8. Radi A, Khalil-Allafi J, Etminanfar M, Pourbabak S., Schryvers D., Amin-Ahmadi B., Influence of stress aging process on variants of nano-$Ni4Ti_3$ precipitates and martensitic transformation temperatures in NiTi shape memory alloy. Materials & Design, 142 (2018) 93–100. https://doi.org/10.1016/j.matdes.2018.01.024
9. Aksöz S, Arslan R, Kardeş N, Sever, Kaplan Y, Bostan B. The Effect of Hot Rolling Temperature on the Wear Properties of NiTi Rods. Transactions of the Indian Institute of Metals, 76 (2023) 951–960. https://doi.org/10.1007/s12666-022-02801-4
10. Tasci U, Yilmaz T, Bostan B., Investigation of microstructure, wear and transverse rupture strength of WE43/nano B4C composites produced by powder metallurgy method, Tribology International, 180 (2023) 108231. https://doi.org/10.1016/j.triboint.2023.108231
11. Luo YC, Li DY. New wear-resistant material: Nano-TiN/TiC/TiNi composite. J Mater Sci, 36 (2001) 4695–4702. https://doi.org/10.1023/A:1017962601833
12. Yang R, Cui L, Zeng Y., Synthesis of TiC/NiTi composite particles by chemical reaction in molten salts, Materials Science and Engineering: A, 438-440 (2006) 1133–1134. https://doi.org/10.1016/j.msea.2006.01.108
13. Jiang H, Cao S, Ke C, Ma X, Zhang X.Y., Nano-sized SiC particle reinforced NiTi alloy matrix shape memory composite, Materials Letters, 100 (2013) 74–77. https://doi.org/10.1016/j.matlet.2013.02.113
14. Farvizi M, Ebadzadeh T, Vaezi M, E.Y. Yoon, Y-J. Kim, H.S. Kim, A. Simchi, Microstructural characterization of HIP consolidated NiTi–nano Al_2O_3 composites. Journal of Alloys and Compounds, 606 (2014) 21–26. http://dx.doi.org/10.1016/j.jallcom.2014.03.184
15. Feng X, Sui J, Cai W, Liu A.I. , Improving wear resistance of TiNi matrix composites reinforced by carbon nanotubes and in situ TiC, Scripta Materialia, 64, 9 (2011) 824–827. https://doi.org/10.1016/j.scriptamat.2011.01.009
16. Zhang Z, Chen D.I., Consideration of Orowan strengthening effect in particulate-reinforced metal matrix nanocomposites: A model for predicting their yield strength, Scripta Materialia, 54, 7 (2006) 1321–1326. https://doi.org/10.1016/j.scriptamat.2005.12.017
17. Casati R, Metals MV., Metal matrix composites reinforced by nano-particles-A Review, Metals, 4, 1 (2014) 65–83. https://doi.org/10.3390/met4010065
18. Bhoi N, Singh H, Materials SP-J of C, Developments in the aluminum metal matrix composites reinforced by micro/nano particles – A review, Journal of Composite Materials, 54, 6 (2020) 813–833. https://doi.org/10.1177/00219983198653
19. Tzamtzis S, Barekar N, Babu N, Processing of advanced Al/SiC particulate metal matrix composites under intensive shearing–A novel Rheo-process, Composites Part A: Applied Science and Manufacturing, 40, 2 (2009) 144–151. https://doi.org/10.1016/j.compositesa.2008.10.017
20. Ray S. Synthesis of cast metal matrix particulate composites. J Mater Sci, 28 (1993) 5397–5413. https://doi.org/10.1007/BF00367809

21. Yang Y, Lan J, Li X., Study on bulk aluminum matrix nano-composite fabricated by ultrasonic dispersion of nano-sized SiC particles in molten aluminum alloy, Materials Science and Engineering: A, 380, 1-2 (2004) 378–383. https://doi.org/10.1016/j.msea.2004.03.073
22. He T, Lu T, Şopu D, Han X, Lu H, et al. Mechanical behavior and deformation mechanism of shape memory bulk metallic glass composites synthesized by powder metallurgy, Journal of Materials Science & Technology, 114 (2022) 42–54. https://doi.org/10.1016/j.jmst.2021.10.002
23. Hosseini Vajargah P, Abdizadeh H, Baghchesara MA. Fabrication of TiB2 nanoparticulates-reinforced aluminum matrix composites by powder metallurgy route. J Compos Mater., 49 (2015) 3115–3125. https://doi.org/10.1177/0021998314560382
24. Sergi A, Khan R, Irukuvarghula S, Meisnar M, Makaya A., Attallah MM, Development of Ni-base metal matrix composites by powder metallurgy hot isostatic pressing for space applications, Advanced Powder Technology, 33, 2 (2022) 103411. https://doi.org/10.1016/j.apt.2021.103411
25. Wąsik A, Leszczyńska-Madej B, Madej M, Rubach R, Garbiec D. Effect of Holding Time on Densification, Microstructure and Selected Properties of Spark Plasma Sintered AA7075-B4C Composites. Materials. 15(6) (2022) 2065. https://doi.org/10.3390/ma15062065
26. Oke SR, Ige OO, Falodun OE, Okoro AM, Mphahlele MR, Olubambi PA. Powder metallurgy of stainless steels and composites: a review of mechanical alloying and spark plasma sintering. International Journal of Advanced Manufacturing Technology, 102, (2019) 3271–3290. https://doi.org/10.1007/S00170-019-03400-2
27. Sabahi Namini A, Delbari SA, Nayebi B, Shahedi Asl M, Parvizi S. Effect of B4C content on sintering behavior, microstructure and mechanical properties of Ti-based composites fabricated via spark plasma sintering. Mater Chem Phys., 251 (2020) 123087. https://doi.org/10.1016/J.MATCHEMPHYS.2020.123087
28. Sadeghi AR, Mostajabodaveh H, Babakhani A, Abravi MS, Salehi A. Effects of milling and heat treatment on the synthesis of NiTi powders. Journal Wuhan University of Technology, Materials Science Edition, 32 (2017) 1156–1162. https://doi.org/10.1007/s11595-017-1725-4
29. Hsieh CT, Ho YC, Wang H, Sugiyama S, Yanagimoto J. Mechanical and tribological characterization of nanostructured graphene sheets/A6061 composites fabricated by induction sintering and hot extrusion. Materials Science and Engineering: A, 786 (2020) 138998. https://doi.org/10.1016/J.MSEA.2020.138998
30. Pillari LK, Lessoway K, Bichler L. Reciprocating dry sliding friction and wear behavior of B319 aluminum alloy-graphene composites. Tribol Int., 192 (2024) 109334. https://doi.org/10.1016/J.TRIBOINT.2024.109334
31. Farvizi M, Ebadzadeh T, Vaezi MR, Kim HS, Simchi A. Effect of nano Al2O3 addition on mechanical properties and wear behavior of NiTi intermetallic. Mater Des., 51 (2013) 375–382. https://doi.org/10.1016/J.MATDES.2013.03.099
32. Hasan MS, Wong T, Rohatgi PK, Nosonovsky M. Analysis of the friction and wear of graphene reinforced aluminum metal matrix composites using machine learning models. Tribol Int. 170 (2022) 107527. https://doi.org/10.1016/j.triboint.2022.107527

33. Chen F, Li Z, Zou LF, Ma WJ, Li JW, Chen Z, et al. Tribological behavior and mechanism of h-BN modified copper metal matrix composites paired with C/C–SiC. Tribol Int, 153 (2021) 106561. https://doi.org/10.1016/j.triboint.2020.106561
34. Saessi M, Alizadeh A, Abdollahi A, Ehsani N. Room temperature wear performance and mechanical properties of hot extruded ultrafine-grained Al5083-5 wt%B_4C-Al2024 tri-modal composites, 6, 9 (2019) 096549. https://doi.org/10.1088/2053-1591/ab2cf3
35. Tang L, Gao C, Huang J, Zhang H, Chang W. Dry sliding friction and wear behaviour of hardened AISI D2 tool steel with different hardness levels. Tribol Int. 66 (2013) 165–173. https://doi.org/10.1016/J.TRIBOINT.2013.05.006
36. Xun L, Ying L, Lu W, Ruoshan L. Ti_2Ni and $TiNi_3$ intermetallic compounds to prepare dense TiNi alloy with enhanced recovery property. Scr Mater. 234 (2023) 115573. https://doi.org/10.1016/j.scriptamat.2023.115573

Сажетак: *У овом раду је циљ био да се побољшају микроструктура, механичка и триболошка својства композитних узорака додавањем 0,25%, 0,5% и 1% нано B4C легури са меморијом облика NiTi. За припрему композитних прахова коришћен је 3Д куглични миксер, а узорци су произведени техником синтеровања у плазми. FE-SEM/EDS и XRD су коришћени за карактеризацију микроструктуре и фаза, наноиндентација за одређивање механичких својстава и уређај за хабање диска за одређивање карактеристика хабања. Утврђено је да се повећањем удела ојачања додатог NiTi, нано B4C керамичке честице таложе на границама зрна и да се вредност тврдоће 1% нано B4C (334 HV) узорка највеће тврдоће значајно повећава за 30% неојачане легуре (264 HV).*

Кључне речи*: микроструктура, механичка својства, композити.*

© 2025 Authors. Published by association for ETRAN Society. This article is an open access article distributed under the terms and conditions of the Creative Commons — Attribution 4.0 International license (https://creativecommons.org/licenses/by/4.0/).